Poly(catechol) modified Fe_3O_4 magnetic nanocomposites with continuous high Fenton activity for organic degradation at neutral pH

Yani Hua
Xi'an Jiaotong University
Chuan Wang (wangchuan@gzhu.edu.cn)
Guangzhou University
Sha Wang
Chongqing Institute of Green and Intelligent Technology
Juan Xiao
Sun Yat-Sen University

Research Article

Keywords: Poly(catechol), Fe3O4 MNPs, Fenton, catalyst, recycle

Posted Date: June 10th, 2021

DOI: https://doi.org/10.21203/rs.3.rs-171416/v1

Version of Record: A version of this preprint was published at Environmental Science and Pollution Research on July 2nd, 2021. See the published version at https://doi.org/10.1007/s11356-021-15088-7.

Abstract

Fe_3O_4 magnetic nanoparticles (MNPs) have been widely used as a recyclable catalyst in Fenton reaction for organic degradation. However, the pristine MNPs suffer from the drawbacks of iron leaching in acidic conditions as well as the decreasing catalytic activity of organic degradation at a pH higher than 3.0. To solve the problems, Fe_3O_4 MNPs were modified by poly(catechol) (Fe_3O_4/PCC MNPs) using a facile chemical co-precipitation method. The poly(catechol) modification improved both the dispersity and the surface negative charges of Fe_3O_4/PCC MNPs, which are beneficial to the catalytic activity of MNPs for organics degradation. Moreover, the poly(catechol) modification enhanced the efficiency of Fe(II) regeneration during Fenton reaction due to the acceleration of Fe(III) reduction by the phenolic/quinonoid redox pair. As a result, the Fenton reaction with Fe_3O_4/PCC MNPs could efficiently degrade organic molecules, exampled by methylene blue (MB), in an expanded pH range between 3.0 and 10.0. In addition, Fe_3O_4/PCC MNPs could be reused up to 8 cycles for the MB degradation with negligible iron leaching of lower than 1.5 mg L^{-1}. This study demonstrated Fe_3O_4/PCC MNPs are a promising heterogeneous Fenton catalysts for organic degradation.

Introduction

Heterogeneous Fenton technique as a promising technique for advanced oxidation processes (AOPs) has been intensively applied for theremoval of organic pollutants because of its intrinsic advantages over classical homogeneous Fenton reactions, including the wide working pH range, no iron sludge pollution, reusable catalysts, and low H_2O_2 consumption(Chen et al., 2017; Goncalves et al., 2020; Luo et al., 2010). Many solid catalysts have been demonstrated to be effective in heterogeneous Fenton reactions(Li et al., 2018; Li et al., 2017). Fe_3O_4 magnetic nanoparticles (Fe_3O_4 MNPs) have received great attention in Fenton reactions(Mondal et al., 2020). The Fe_3O_4 MNPs possess unique properties, magnetism, which can be effectively separated from the solution using a magnetic field (Mercado et al., 2018; Magnacca et al., 2014). Especially, Gao et al. demonstrated that Fe_3O_4magnetitenanoparticles possessed an intrinsic enzyme mimetic activity similar to that of peroxidases in nature, which were widelyused to oxidize organic pollutant in the treatment of wastewater. Further, Fe_3O_4 MNPs possessed highly effectivecatalyticactivity, which possessed ahigher binding affinity for the substrate TMB than HRP and exhibiteda40-fold higher level of activity at the same molar catalyst concentration than that of HRP (Gao et al., 2007).Moreover, the Fe(II) in Fe_3O_4 MNPs plays an important role as the electron donor to initiate the Fenton reactions. The octahedral sites in the magnetite structure can accommodate both Fe(II) and Fe(III)simultaneously. Hence the reversible transformation of Fe(II)/Fe(III) can happen within the same structure during Fenton reaction (Wang et al., 2020; Wang et al., 2010), that is to say, Fe(III) transforms to Fe(II) and Fe(II) continues to catalyze H_2O_2. Thus, Fe_3O_4 MNPs can be used as Fenton catalysts for activating H_2O_2(Cai et al., 2021; Xiang et al., 2021).

However, the iron leaching from the Fe_3O_4 MNPs at acidic pH and the low catalytic activity at neutral and alkaline pH could affect the stability and activity of Fe_3O_4 MNPs, thus limiting their applications (Pu et al., 2014). Previous studies have shown, that, for the degradation of 2,4-dichlorophenol (2,4-DCP) with Fe_3O_4 MNPs, 9.8 mg L^{-1} of Fe dissolved into the solution at pH 3.0 after 180 min. Slow degradation of 2,4-DCP was observed at a pH values of 3.9, 4.6 and 5.0, although a lower pH caused a shorter induction time and a higher kinetic rate (Xu et al., 2012). Dimethyl phthalate (DMP) was quickly removed in the acidic solution with pH range from 3.0 to 4.5. However, at pH 8.0, the Fe_3O_4 MNPs had very little activity as Fenton catalysts (He et al., 2015). The low catalytic activity at high pH values is mainly caused by the oxidation of these fine particles with limited Fe(II) regeneration during heterogeneous Fenton processes. Hu et al. reported that the Fe(II) amount in the total surface Fe atoms of Fe_3O_4/MWCNTs for used and fresh catalysts were 13.3% and 31.7%, respectively (Hu et al., 2013). Many efforts have been paid to improving the catalytic performance of Fe_3O_4 MNPs (Hammouda et al., 2015). Niu et al. introduced humic acid (HA) to coat Fe_3O_4 magnetic nanoparticles, i.e., Fe_3O_4/HA, which exhibited a high catalytic ability for H_2O_2 decomposition. This was caused by rapid electron transfer among the complexed Fe(II)-HA and Fe(III)-HA, leading to the rapid regeneration of Fe(II) species and the fast production of •OH radicals (Niu et al., 2011).

Organic ligands (citrate, oxalate, ethylenediaminetetraacetic acid, etc.) have been used to modify the surface of iron compounds to control their solubility in Fenton or Fenton-like processes (Bai et al., 2013; Baldi et al., 2010; Jho et al., 2012). Among those iron ligands, catechol, could form strong coupling with the iron ions which reduced the Fe^{3+}/Fe^{2+} redox potential (Niu et al., 2011; Kang et al., 2009). In addition, catechol can directly reduce Fe(III) to Fe(II), which itself transformed to the corresponding quinones (Melin et al., 2015). Therefore, introducing catechol in Fenton or Fenton-like processes can widen the reaction pH to neutral conditions by preventing iron from precipitation and, at the same time, enhance the electron transfer (Chen et al., 2017; Contreras et al., 2009). However, it also contributes a certain amount of total organic carbon (TOC) that consumes a certain amount of H_2O_2 in a Fenton system. Finally, catechol will be degraded and exhausted, which will result in the degradation of the catalytic performance (Xiao et al., 2016).

The polymerization of catechol, catalyzed by Fe(III), forms poly(catechol) (Elhabiri et al., 2007; Gulley-Stahl et al., 2010; Slikboer et al., 2015). Poly(catechol), containing phenolic/quinonoid redox-active units in the main chain, is a redox-active polymer. Moreover, the binding of the bidentate enediol ligands from the catechol group converted the under-coordinated iron on the surface sites back to a bulk-like lattice structure with an octahedral geometry for the oxygen-coordinated iron, which consequently ended up with tight binding between ligands and iron oxide (Xu et al., 2004). Poly(catechol) has been exploited as adhesives and coatings on the surfaces of oganic and inorganic materials due to their unique thermal, structural properties, and the ability to form strong charge transfer complexes with the metal oxides (Faure et al., 2013; Ye et al., 2011). Therefore, we propose that Fe_3O_4 MNPs modified with poly(catechol) will greatly increase the catalytic activity of Fe_3O_4 MNPs without sacrifice the structural stability. The

introduction of poly(catechol) in Fe_3O_4/PCC MNPs could offer the following advantages: i) preventing nanoparticles from agglomeration and broadening the working pH range of Fenton reactions; ii) avoiding Fe(II) oxidation and iron leaching; iii) accelerating the Fe(III)/Fe(II) conversion with the recyclable organic ligands.

In this work, Fe_3O_4/PCC MNPs were prepared by a facile co-precipitation method. The obtained material was tested for heterogeneous Fenton degradation of MB, used as a model organic pollutant. The structure, surface charge, electron transfer ability, and catalytic activity of Fe_3O_4/PCC MNPs were investigated. The possible mechanisms for Fe_3O_4/PCC MNPs formation and enhanced MB degradation were also proposed.

Experimental Section

Chemicals

All chemicals were analytical grade and used without further purification. Ferric chloride ($FeCl_3{\cdot}6H_2O$), ferrous sulfate ($FeSO_4{\cdot}7H_2O$), hydrogen peroxide (H_2O_2, 30 wt.%), ammonium hydroxide ($NH_3{\cdot}H_2O$, 25%), methylene blue (MB), methyl orange (MO), and catechol were obtained from Chuandong Chemical Inc., Chengdu, Sichuan, China. 5,5’-dimethyl-1-pirroline-N-oxide (DMPO) and 4-chloro-7-nitrobenz-2-oxa-1,3-diazole (NBD-Cl) were purchased from Adamas, Shanghai, China.

Preparation and characterization of catalysts

Fe_3O_4/PCC MNPs were prepared by a facile chemical co-precipitation method using iron salts and catechol as precursors (Wang et al., 2014). In brief, $FeCl_3{\cdot}6H_2O$ (10 mmol) and $FeSO_4{\cdot}7H_2O$ (5 mmol) were dissolved into 75 mL deionized water, before adding 75 mL of catechol aqueous solution (1.5 mM). The mixture was also used as the poly(catechol) precursor. The solution was standing for 30 min before adding into 100 mL of ammonium hydroxide (3.3 M) rapidly. The solution was aged for 120 min under vigorous stirring. The whole synthesis processes were performed in an ambient atmosphere. The black magnetic nanoparticles were separated by an external magnet and were washed with deionized water until pH neutral. The collected nanoparticles powder was dried in a vacuum oven at 50°C for 24 h to obtain Fe_3O_4/PCC MNPs. The pristine Fe_3O_4 MNPs without PCC were synthesized following the same procedure without adding catechol. The poly(catechol)-Fe was obtained following the same procedure without adding ammonium hydroxide. All the products were stored in a desiccator under ambient temperature for further experiments.

The morphology and size distribution of Fe_3O_4/PCC and Fe_3O_4 MNPs were obtained from a transmission electron microscope (TEM, Tecnai™ G2 Spirit, FEI, USA). The phase structures of the Fe_3O_4/PCC and Fe_3O_4 MNPs were determined by X-ray diffraction (XRD, Empyrean, Netherlands) and Raman spectroscopy (Renishaw, inVia Qontor, Germany). To verify the formation of poly(catechol), the surface

chemistry of catechol, poly(catechol), Fe_3O_4 and Fe_3O_4/PCC MNPs were analyzed using fourier transform infrared (FTIR) spectrometer (Cary 630, Agilent). The FTIR samples were prepared in pressed KBr pellets. The interaction between Fe_3O_4 and poly(catechol) was analyzed using x-ray photoelectron spectroscopy (XPS, ESCALAB 250, ThermoVG Scientific, USA) with Al Kα (1486.6 eV) as the x-ray source. All XPS spectra were corrected using the C 1s line at 284.6 eV. Thermal stability of Fe_3O_4 and Fe_3O_4/PCC were performed by a thermogravimetric analyzer (TGA, TGA/DSC 1, Mettler-Toledo, Switzerland). The tests were performed at heating rate of 5°C min^{-1} from room temperature to 1000°C under the nitrogen flow, and the weight retention-temperature curves were recorded. The zeta potentials of the catalyst suspensions at different pH values were determined by an analyzer (Zetasizer, Malvern 3000). The electron transfer ability of the catalysts was examined by cyclic voltammetry measurements using an electrochemical workstation (CHI660, CH Instruments, Chenhua, Shanghai, China) in a cell with a three-electrode configuration. Glassy carbon electrodes deposited with Fe_3O_4 or Fe_3O_4/PCC MNPs respectively were used as working electrodes. A Pt foil and a saturated calomel electrode (SCE) were used as the anode and the reference electrode, respectively. The measurements were carried out in the potential range of 0 to 1.0 V versus Hg/HgO at a scan rate of 10 mVs^{-1}.

Degradation procedures

The degradation procedures were carried out in a beaker (100 mL) shaken at a speed of 180 rpm. In a typical reaction, MB solution (50 mL) with a certain concentration was prepared with the addition of the specified amount of Fe_3O_4/PCC MNPs. The pH of the reaction solution was adjusted to a required value using H_2SO_4 (1.0 M) or NaOH (1.0 M) solution. The degradation reactions were initiated by adding H_2O_2 to the suspension once the adsorption equilibrium was achieved. At different time intervals, a suspension sample (0.6 mL) was collected and the reaction was immediately quenched with the solution of pure methanol (30 µL). The solid samples were separated from the solution using an external magnet. The supernatant liquid was collected for analysis. To test the stability of Fe_3O_4/PCC composites, the catalyst was gathered via an external magnet, followed by washing, and drying under vacuum, and then reused in a fresh solution of MB and H_2O_2 several times. Each experiment was run in triplicate, and average values and standard deviations are presented.

Analytical methods

The MB concentration was measured by UV-vis spectroscopy at the maximum absorption wavelength of MB (660 nm) (Anelise L. et al. 2012; Banerjee S. et al. 2018; Li K.Y. et al. 2017). The MB mineralization was evaluated by an total organic carbon (TOC) analyzer (MultiN/C3100TOC/TN, Analyticjena, AG). The total carbon content on the catalyst was measured by the elemental analyzer (Vario EL cube). The total leached iron was measured using the orthophenantroline complexometric method (λ = 510 nm). The formation of $\bullet O_2^-$ was determined by a fluorescence method using 4-chloro-7-nitrobenz-2-oxa-1,3-diazole (NBD-Cl) as a radical scavenger. The concentration of the reaction product between $\bullet O_2^-$ and NBD-Cl was measured with a fluorescence spectrometer (Hitachi F-4600, Hitachi, Japan) at the emission of 550 nm with the excitation of 470 nm. •OH radicals were identified by electron spin resonance spectroscopy (ESR,

ESP 300E, Bruker), operating at the center field strength of 3514 G with 9.85 GHz microwave frequency. For electron spin resonance (ESR) assay, samples (0.5 mL) were taken instantaneously after 20 min into the heterogeneous Fenton reaction. The samples were mixed with 50 µL of DMPO (500 mM) to form the DMPO-OH adduct. The ESR spectra of the reaction filtrate were recorded.

Results And Discussion

Formation of Fe_3O_4/PCC MNPs

Scheme 1 shows the formation processes of Fe_3O_4/PCC MNPs. The polymerization of catechol was catalyzed by Fe^{3+} in the mixed solution, forming blank coarse precipitates containing poly(catechol) (Slikboer et al., 2015). Simultaneously, some Fe^{3+} ions were chemically adsorbed on the poly(catechol) precipitates through complexation and served as the nucleation centers for the subsequent growth of Fe_3O_4 once ammonium hydroxide was added. The formed Fe_3O_4/PCC chains entangled with each other to form the Fe_3O_4/PCC MNPs. The weight average molecular of poly(catechol) obtained from the polymerization of catechol catalyzed by Fe^{3+} was 817 g mol^{-1}.

Characterization of Fe_3O_4/PCC MNPs

The FTIR spectra of catechol, poly(catechol), Fe_3O_4 and Fe_3O_4/PCC MNPs were shown in Fig. 1a. The peak at 584 cm^{-1} is ascribed to the stretching vibrations of the Fe-O bond in the spectra of Fe_3O_4 and Fe_3O_4/PCC MNPs (Leng et al., 2013). The v_{OH} peak at 3326 cm^{-1} from the catechol disappeared from the poly(catechol) and Fe_3O_4/PCC MNPs (Kong et al., 2002), which indicated the polymerization of catechol, and catechol retained only one hydroxyl group during the polymerization processes, being consistent with the reports in the literature (Dubey et al., 1998). The peak at 1280 cm^{-1} from the Fe_3O_4/PCC MNPs and poly(catechol), is attributed to the asymmetrical stretching of C-O-C_{arom} and C-OH (Dubey et al., 1998). The peaks observed at 1400 cm^{-1}, 1460 cm^{-1}, can be assigned to the stretch of C-C, C = C in the aromatic ring (Aktas et al., 2003), which demonstrates that organic ligand indeed existed in the magnetic nanocomposites.

The XRD patterns of Fe_3O_4/PCC and pristine Fe_3O_4 MNPs are shown in Fig. 1b. The diffraction peaks at 2θ at 30.3°, 35.6°, 43.3°, 53.7°, 57.2°, 62.7° were observed from both samples. These peaks are assigned to the (220), (311), (400), (422), (511), and (440) planes of the cubic spinel structure of Fe_3O_4 (PDF#65-3107). The similarity of the dominant XRD patterns indicates that the presence of poly(catechol) did not affect the crystal structure of Fe_3O_4 (Mercado et al., 2018; Mercado et al., 2018; Mercado et al., 2014; Mercado et al., 2018). The Fe_3O_4 MNPs in the composites are highly pure Fe_3O_4 phase with an inverse spinel structure since no XRD peaks from other magnetite were detected (Hu et al., 2011). Moreover, the structural characteristics of Fe_3O_4, Fe_2O_3 and Fe_3O_4/PCC MNPs were characterized by Raman

spectroscopy (Fig.S1a). As shown as Fig.S1a, the Raman spectroscopy of Fe_3O_4 and Fe_2O_3 were very similar, and it was possible to distinguish hematite domains might be present. Nevertheless, the reason might be the oxidation of Fe(II) to Fe(III) during the Raman test, according with the published study that in-situ laser oxidation might take place (Jubb et al., 2010). From the hysteresis loop of Fe_3O_4 and Fe_3O_4/PCC MNPs (Fig.S1b), there were no coercive force and residual magnetism in Fe_3O_4 and Fe_3O_4/PCC MNPs, indicating the magnetic separation characteristic of Fe_3O_4/PCC MNPs (Mercado et al., 2018; Magnacca et al., 2014).

To characterize the morphology and size distribution of Fe_3O_4/PCC and Fe_3O_4 MNPs, TEM images were obtained from a transmission electron microscope. The TEM and HRTEM images of Fe_3O_4 and Fe_3O_4/PCC MNPs were illustrated in Fig. 1c, Fig. 1e and Fig. 1d, Fig. 1f, respectively. As shown as Fig. 1c and Fig. 1d, both Fe_3O_4 and Fe_3O_4/PCC MNPs were in a quasi-spherical in shape and the average particle size of Fe_3O_4 and Fe_3O_4/PCC MNPs were 8.06 nm and 6.32 nm, respectively. According to the formation processes of Fe_3O_4/PCC MNPs, there were a large number of phenolic hydroxyl groups distributed around Fe_3O_4 nanoparticles due to the modification of poly(catechol), and the ionization of phenolic hydroxyl groups made the composites negatively charged, which promoted the repulsion between nanoparticles and prevented them from agglomerating, thus availed to improve the dispersity of Fe_3O_4/PCC nanoparticles. Therefore, Fe_3O_4/PCC MNPs were much more dispersed than those of Fe_3O_4 MNPs. This observation suggested that poly(catechol) in the catalysts could prevent the agglomeration of nanoparticles indeed. As presented in Fig. 1e and Fig. 1f, the measured d-spacings equal to 0.251 nm and 0.209 nm were assigned to the lattice spacing of the (311) and (400) plane of Fe_3O_4 and Fe_3O_4/PCC, respectively, which was accordance with the results of XRD patterns.

Figure 2a shows the XPS spectra of the MNPs. The dominant peaks at the binding energies of ~ 285, 530, and 711 eV are ascribed to the C 1s, O 1s, and Fe 2p, respectively. Figure 2b shows the high resolution Fe 2p spectra of Fe_3O_4 and Fe_3O_4/PCC MNPs. The peaks from the Fe 2p1/2 and Fe 2p3/2 are located at 710.8 and 724.5 eV, respectively. The results are consistent with the literature data for magnetite, which confirmed the successful formation of Fe_3O_4 (He et al., 2011). Moreover, 32.6% of the total surface iron atoms were in the Fe(II) state in Fe_3O_4/PCC MNPs (Fig. S2a). This is much higher than that in the pristine Fe_3O_4 MNPs (25%, Fig. S2b), which was due to the complexation and reduction of irons by the poly(catechol) in the Fe_3O_4/PCC MNPs. The O 1s spectrum of Fe_3O_4/PCC MNPs is shown in Fig. 2c. The deconvolution of the O 1s spectra revealed four peaks: (i) the oxygen that belonging to lattice oxygen in the Fe_3O_4 (Fe-O: 530.2 eV), (ii) the oxygen from the Fe-O-C bonds (530.5 eV) associated with possible bidentate coordination between the surface Fe and phenolic hydroxyl group of Fe_3O_4/PCC MNPs, (iii) the oxygen from the hydroxy groups (-OH: 531.5 eV) and (iv) the oxygen in epoxy and hydroxyl group (C-O-C, C-O: 532.9 eV (Zubir et al., 2014). The deconvolution of the C 1s spectra (Fig. 2d) of Fe_3O_4/PCC also consisted of four peaks: C = C (284.6 eV), C-C (285.2 eV), C-O (286.3 eV), and C = O (288.9 eV) (Chandra et al., 2010), indicating the existence of quinone in the Fe_3O_4/PCC.

Figure 3a shows the zeta potentials of the catalyst suspensions at varied pH values. The point of zero charge (PZC) of Fe_3O_4 MNPs was 4.2, while the surface of Fe_3O_4/PCC MNPs was negatively charged in the pH range of 2.0 to 10.0, which could be caused by the electronegativity of the phenolic hydroxyl group in poly(catechol). Moreover, the surface charge density of Fe_3O_4/PCC MNPs increased with the increasing pH.

The thermal behaviors of Fe_3O_4 and Fe_3O_4/PCC MNPs were further investigated by the TGA analysis shown in (Fig. 3b). The Fe_3O_4/PCC MNPs showed weight loss at the temperature below 150°C, caused by the loss of physically adsorbed water. The weight loss observed from 150°C to 450°C is ascribed to the loss of oxygen-containing functional groups. The final weight loss happening from 450°C to 800°C is mainly attributed to the complete decomposition of organic residues (Zhang et al., 2015). Comparing with the poly(catechol)-Fe complexes, it can be found that the weight loss of the Fe_3O_4/PCC MNPs is greatly restrict, indicating strong complexation between Fe_3O_4 and poly(catechol). For Fe_3O_4, a slight weight gain below 400°C is due to the oxidization of Fe_3O_4 to γ-Fe_2O_3 (Xie et al., 2012). From the TGA curve, the fraction of the organic component in Fe_3O_4/PCC composites (red) was estimated to be 13 wt% (Li et al., 2008).

Heterogeneous Fenton catalytic activity of Fe_3O_4/PCC MNPs

Comparison of catalytic activity

The catalytic activity of both Fe_3O_4 and Fe_3O_4/PCC MNPs (1.0 g L^{-1}) were evaluated based on the degradation of MB (0.1 mM) with H_2O_2 (40.0 mM) at an initial pH of 6.0 (Fig. 4a). No significant degradation of MB was observed in the presence of only 40 mM H_2O_2 without any catalyst. Similarly, less than 10% of MB was removed in the Fe_3O_4 suspension with or without the addition of H_2O_2. However, 63% of MB was adsorbed onto Fe_3O_4/PCC MNPs and nearly 100% of MB was removed in the presence of H_2O_2 catalyzed by Fe_3O_4/PCC MNPs within 120 min. The results indicated that Fe_3O_4/PCC MNPs exhibited a higher adsorption capacity and stronger catalytic activity for H_2O_2 decomposition than those of Fe_3O_4 MNPs due to the introduction of poly(catechol) in Fe_3O_4/PCC MNPs.

In the Fe_3O_4/PCC MNPs catalyzed MB degradation process, MB was first enriched at the vicinity of the catalyst surface through the electrostatic adsorption, which was due to the facts that the poly(catechol) modification increased the surface negative charges of Fe_3O_4/PCC MNPs (Fig. 3a) and improved the dispersity of the nanoparticles (Fig. 1d). The adsorbed MB could be much easier to be oxidized by the hydroxyl radicals generated on the surface of Fe_3O_4/PCC MNPs since the organic pollutant adsorbed on the surface of catalysts are much more reactive (Xue et al., 2009; Noorjahan et al., 2005; Gu et al., 2013). The adsorption of MB on the Fe_3O_4/PCC MNPs was quantitatively studied and shown in Fig. S3 and Fig.

S4 (in supporting information: S1.1 and S1.2). In contrast, methyl orange (MO), an anion dyes, was neither adsorbed on the Fe_3O_4/PCC MNPs nor degraded after the addition of H_2O_2 shown in Fig. S5 (in supporting information: S2). This confirmed that the degradation of MB was initiated by the adsorption of MB on Fe_3O_4/PCC MNPs. A similar effect was found by Gu et al. that a magnetic porous carbon derived from the sludge showed a highly active property as an efficient heterogeneous catalyst to adsorb and degrade naphthalene dye (1,2,4-Acid) in an aqueous solution through a Fenton-like reaction (Gu et al., 2013).

In addition, poly(catechol), coordinated with Fe(III) on the surface of Fe_3O_4/PCC MNPs, could facilitate the Fe(II)/Fe(III) conversion by the phenolic/quinonoid redox pair during the Fenton reaction (Feng et al., 2016). To better evaluate the catalytic activity of the catalyst, cyclic voltammetry measurements were adopted, which were shown in Fig. 4b. The cathodic and anodic peaks can be attributed to the reduction of Fe(III)/Fe(II) and the oxidation of Fe(II)/Fe(III), respectively. In comparison with Fe_3O_4 MNPs, both the cathodic and the anodic peaks of Fe_3O_4/PCC MNPs shifted towards smaller potentials, which indicated that the Fe(III)/Fe(II) redox reactions became more easily with the presence of PCC. The peak potential difference between the cathodic and anodic peaks of Fe_3O_4/PCC MNPs (92 mV) was also smaller than that of Fe_3O_4 MNPs (280 mV), which confirmed the acceleration of the Fe(III)/Fe(II) redox cycling with the introduction of poly(catechol). The fast Fe(II) regeneration can greatly promote the degradation of MB in the heterogeneous Fenton system (Ma et al., 2015).

Effect of initial pH on the catalytic activity of Fe_3O_4/PCC MNPs

Figure 5 shows the effect of initial pH on the degradation of MB with Fe_3O_4/PCC MNPs. Nearly 100% of MB was removed within 120 min in an expanded pH range of 3.0 to10.0. Based on the first-order kinetics, the degradation rate constant, *k*, slightly decreased with the increase of pH. This was quite different from some Fe_3O_4-based degradation system, in which the removal efficiency decreased sharply as the solution pH increased (Zhang et al., 2014; Zhang et al., 2014; Wang et al., 2012). On one hand, MB was more easily enriched at the vicinity of the catalyst surface with the increase of pH maintaining fast oxidation. On the other hand, poly(catechol) enhanced the Fe(II) regeneration in the Fenton reaction with Fe_3O_4/PCC MNPs due to the acceleration of the Fe(II)/Fe(III) recycling (Fig. 4b). Hence, the Fe_3O_4/PCC MNPs became less sensitive to the solution pH.

The amount of iron leaching from the catalyst was as low as 1.02 mg L^{-1}, 0.62 mg L^{-1}, 0.37 mg L^{-1} and 0.49 mg L^{-1}, at the pH of 3.0, 6.0, 9.0, and 10.0, respectively. The possible reason for the negligible iron leaching was that the phenolic hydroxyl groups at the surface of the Fe_3O_4/PCC MNPs were hydrolyzed to form a thin layer of H^+, which could prevent the diffusion of H^+ into the Fe_3O_4. Thus Fe_3O_4/PCC MNPs were stable even at acidic conditions.

Mineralization of MB and •OH radicals detection

Under our reaction conditions, MB concentration was decreased monotonically in the Fenton-like degradation process within 120 min (see in supporting information: S3, Fig. S6). To evaluate the mineralization of MB, the total carbon concentration (TOC) was measured. The total organic content was increased by 0.24 mg after the first circle of Fenton-like degradation with Fe_3O_4/PCC MNPs. This value was increased to 1.57 mg after eight reaction cycles. In each reaction cycle, 0.1 mM 50 mL of MB (0.995 mg carbon) was added to the system. The net TOC removal was obtained by calculating the TOC difference coming from both the solid catalyst and liquid solution before and after the degradation reactions. Hence, during the first reaction cycle, 48.3% of TOC was mineralized using 1.0 g L^{-1} Fe_3O_4/PCC MNPs and 40 mM H_2O_2 at pH 6.0 and 30°C within 120 min. After eight cycles, TOC removal efficiency was maintained at 40.7% (Table 1).

Table 1
TOC removal efficiency of the system ($[Fe_3O_4/PCC]$ = 1.0 g L^{-1}, $[H_2O_2]_0$ = 40 mM, $[MB]_0$ = 0.1 mM, pH 6.0, T = 30°C, t = 120 min/recycling)

	The carbon content (mg)	
	The carbon content of catalysts	The carbon content of MB in the solution
Before reaction	4.230	0.995
After 1st reaction	4.470	0.274
After 2st reaction	-	0.476
After 3st reaction	-	0.496
After 4st reaction	-	0.542
After 5st reaction	-	0.424
After 6st reaction	-	0.301
After 7st reaction	-	0.324
After 8st reaction	5.803	0.312
TOC removal efficiency (After 1st cycle) (%)	48.3	
TOC removal efficiency (After 8st cycle) (%)	40.7	

To identify the reactive oxygen species (ROS) responsible for the mineralization of MB, the concentrations of •OH and $•O_2^-$ were detected by ESR and fluorescence method, respectively, during the MB degradation (Ma et al., 2015; Zhang et al., 2014). DMPO and NBD-Cl were used as the probes for the determination of •OH and $•O_2^-$ respectively. As shown in Fig. 6a, $•O_2^-$ was produced in the presence of Fe_3O_4 and Fe_3O_4/PCC MNPs. The amount of $•O_2^-$ in the presence of Fe_3O_4/PCC MNPs was increased sharply within the initial 5 min and then reached a plateau, which was lower than that of the pristine

Fe_3O_4 MNPs. The result suggested that $\bullet O_2^-$ is not responsible for the enhanced degradation of MB with Fe_3O_4/PCC MNPs.

The ESR spectra in the presence of Fe_3O_4 MNPs and Fe_3O_4/PCC MNPs displayed a fourfold characteristic peak of the typical DMPO-•OH adduct with the intensity ratio of 1:2:2:1. No significant decrease in the ESR signal after the sixth repeated run of MB degradation with Fe_3O_4/PCC MNPs (Fe_3O_4/PCC-6st MNPs).However, the intensity of •OH in the Fe_3O_4/PCC-H_2O_2 system was much higher than that of the Fe_3O_4-H_2O_2 system (Fig. 6b). The results indicated that the addition of poly(catechol) in Fe_3O_4/PCC MNPs enhanced the transformation of H_2O_2 into •OH radicals. It confirmed that •OH radicals were the main active species involved in the process of MB degradation (Wang et al., 2020; Wang et al., 2010), which is also responsible for the stable performance of the Fe_3O_4/PCC MNPs catalyst.

Stability of Fe_3O_4/PCC MNPs

Stability is an important property for an effective catalyst. To evaluate the stability of the catalyst, eight reaction cycles for MB removal with Fe_3O_4/PCC MNPs (1.0 g L^{-1}) were continuously performed using 40.0 mM H_2O_2 at pH 6.0 and 30°C. Each cycle lasted 120 min. After each reaction, Fe_3O_4/PCC MNPs were separated from the reaction solution with a powerful magnet and rinsed with distilled water three times before reused in the next Fenton processes. During the eight times recycling, MB was almost completely removed with negligible iron leaching (< 1.5 mg L^{-1}) (Fig. 7). This is consistent with the fact that there was no significant decrease in the concentration of •OH radicals produced after six cycles of running (Fig. 6b), which was due to the enhanced Fe(II) regeneration. The results demonstrated the good stability and high catalytic activity of the Fe_3O_4/PCC MNPs.

Since the reduction of Fe(III) to Fe(II) is crucial for the continuous generation of •OH, the amount of surface Fe(II) on the catalyst after the reaction was investigated using XPS analysis shown in Fig. 8a. The survey spectrum from the used Fe_3O_4/PCC MNPs exhibited peaks at the binding energies of 285, 530 and 711 eV, which were ascribed to C 1s, O 1s, and Fe 2p respectively. Figure 8b shows the details of the Fe 2p peaks (Fe $2p_{1/2}$ and Fe $2p_{3/2}$) of used Fe_3O_4/PCC MNPs. The Fe $2p_{3/2}$ peak was deconvoluted into three components at 713.42 eV, 711.30 eV, and 710.03 eV, which were assigned to the $Fe(III)_{tct}$, $Fe(II)_{oct}$ and $Fe(II)_{oct}$, respectively. About 34.8% of the total surface iron atoms were in the Fe(II) state in Fe_3O_4/PCC MNPs after MB degradation, close to the fresh catalyst (32.6%). This was different from some studies which observed that the amount of Fe(II) declined gradually during the Fenton reaction (Hu et al., 2011). The stable concentration of Fe(II) is associated with the presence of poly(catechol) which accelerated the reduction of Fe(II) driven by the phenolic/quinonoid conversion. Moreover, the chemical stability of poly(catechol) makes itself resilient against degradation due to the steric hindrance. Hence, it could contribute to the repeated effective catalytic performance of Fe_3O_4/PCC MNPs at neutral pH. The

stable catalytic efficiency, negligible iron species leaching, as well as convenient recycling of Fe_3O_4/PCC MNPs, made it an attractive catalyst for the Fenton reactions.

Possible mechanism for activating H_2O_2 using Fe_3O_4/PCC MNPs

Since •OH radicals were the main active species involved in the degradation of MB, it is essential to figure out whether the •OH radicals generated by the homogeneous catalytic reaction is also contributed. The homogeneous Fenton reactions were performed in 3.0 mg L^{-1} $FeSO_4 \cdot 6H_2O$ solution. We chose this concentration since it is higher than the maximal amount of total iron leached from the Fe_3O_4/PCC MNP catalyst after the oxidation cycles. Only less than 10% of MB dagradation was achieved in the homogeneous Fenton process with 40 mM H_2O_2 at pH 6.0 and 30°C within 120 min, which indicated the importance of the solid state Fe_3O_4/PCC in the heterogeneous decomposition of MB (Dong et al., 1995; Rahhal et al., 1988).

The mechanism for the MB degradation with activated H_2O_2 in the heterogeneous Fenton reaction on Fe_3O_4/PCC MNPs is proposed in Scheme 2. Firstly, MB was adsorbed on Fe_3O_4/PCC MNPs through electrostatic adsorption (Scheme 2a). Then, H_2O_2 was activated on the surface of Fe_3O_4/PCC MNPs to produce •OH radicals for MB degradation (Scheme 2b). The adsorption of MB was beneficial to its degradation as discussed above. That the presence of quinones in PCC also improve the degradation of organic compounds in the Fenton processes, due to their role as an electron shuttle (Kang et al., 2009; Fang et al., 2013). The poly(catechol) in Fe_3O_4/PCC MNPs introduced the phenolic/quinonoid redox cycle, which in turn accelerated the Fe(III)/Fe(II) cycle (Chen et al., 2017; Leng et al., 2013). This enhanced Fe(II) regeneration during the Fenton reaction (Fig. 4b) helped to maintain the high catalytic activity of Fe_3O_4/PCC MNPs in a wide pH range. The improved Fe(II) regeneration by poly(catechol) was verified by the XPS results (Fig. 8b).

In the Fenton reactions on Fe_3O_4/PCC MNPs, the surface Fe(II) from the Fe_3O_4/PCC MNPs catalyzed the decomposition of H_2O_2 to form the •OH radicals (Reaction 1) which were reactive for the degradation and mineralized of MB (Reaction 2). Simultaneously, H_2O_2 reacted with the surface Fe(III) to produce Fe(II) and $\bullet O_2^-$ (Reaction 3) (Wang et al., 2014; He et al., 2014). The produced $\bullet O_2^-$ was rapidly consumed by Fe(III) reduction (Reaction 4). Meanwhile, Fe(III) could also be quickly reduced to Fe(II) by poly(catechol) and semiquinone radicals (SQ) (Reactions 5 and 6), which were essential for the generation of •OH radicals through Reaction 1 (Leng et al., 2014). As the cycles increased, the quinone analogues were accumulated continuously in the system, forming more Fe(II) and •OH radicals. Hence, the MB degradation was accelerated. Therefore, Fe_3O_4/PCC MNPs exhibited a stable and high catalytic activity for the decomposition of organic molecules by H_2O_2.

$\equiv Fe(II) + H_2O_2 \rightarrow \equiv Fe(III) + \cdot OH$ (1)

$\bullet OH + MB \rightarrow$ intermediates $\rightarrow$Degraded/mineralized product (2)

$\equiv Fe(III) + H_2O_2 \rightarrow \equiv Fe(II) + \cdot O^{2-}$ (3)

$\equiv Fe(III) + \cdot O^{2-} \rightarrow \equiv Fe(II) + O_2$ (4)

$Phenolic + \equiv Fe(III) \rightarrow SQ + H^+ + \equiv Fe(II)$ (5)

$SQ + \equiv Fe(III) \rightarrow Quinonoid + \equiv Fe(II) + H^+$ (6)

Conclusion

Poly(catechol) modified Fe_3O_4 MNPs (Fe_3O_4/PCC MNPs) were successfully synthesized by a facile coprecipitation method. The coupling of Fe_3O_4 MNPs with poly(catechol) has improved the dispersity of the MNPs due to the negative surface charges. Such highly dispersed MNPs have improved the kinetics for the degradation of MB. Moreover, poly(catechol) in the catalyst accelerates the Fe(III)/Fe(II) recycling, which increases the generation of •OH radicals that are the dominant oxidant in the Fenton reactions for MB degradation in a wide pH range of 3.0–10.0. The negligible iron leaching, the enhanced Fe(II) regeneration, and the refractory degradation of poly(catechol) have all contributed positively to the good stability and high activity of Fe_3O_4/PCC MNPs. This work provides a new pathway for preparing a heterogeneous Fenton catalyst with potential applications in wastewater treatment.

Declarations

Competing interests

The authors declare that they have no competing interests.

Ethical approval Not applicable.

Consent to publish Not applicable.

Consent to participate

Not applicable.

Authors'Contributions NH conducted the experiment and experimental analysis, contributed to the discussion of the study, and wrote the original draft of the manuscript. CW supervised the research, conducted the experimental analysis, funding acquisition, and reviewed and edited the manuscript. SW and JX contributed to the discussion of the study and wrote the original draft of the manuscript.

Funding The present research supported by the Natural Science Foundation of China (No. 51678554,No. 51978181).

Data availability All data generated or analyzed during this study are included in this published article and its supplementary information files.

References

1. Aktas N, Sahiner N, Kantoglu O, Salih B, Tanyolac A (2003) Biosynthesis and characterization of laccase catalyzed poly(catechol). J Polym Environ 11:123–128
2. Bai C, Xiao W, Feng D, Xian M, Guo D, Ge Z, Zhou Y (2013) Efficient decolorization of Malachite Green in the Fenton reaction catalyzed by [Fe(III)-salen]Cl complex. Chem Eng J 215–216:227–234
3. Baldi Marchetto F, Zanchettin D, Sartorato E, Paganelli S, Piccolo O (2010) A bio-generated Fe(III)-binding exopolysaccharide used as new catalyst for phenol hydroxylation. Green Chem 12:1405–1409
4. Cai HD, Li X, Ma DC, Feng QG, Wang DB, Liu Z, Wei X, Chen K, Lin HY, Qin SY, Lu FY (2021) Stable Fe_3O_4 submicrospheres with SiO_2 coating for heterogeneous Fenton-like reaction at alkaline condition. Sci Total Environ 764:144200–144200
5. Chen F, Xie S, Huang X, Qiu X (2017) Ionothermal synthesis of Fe_3O_4 magnetic nanoparticles as efficient heterogeneous Fenton-like catalysts for degradation of organic pollutants with H_2O_2. J Hazard Mater 322:152–162
6. Chandra V, Park J, Chun Y, Lee JW, Hwang IC, Kim KS (2010) Water-dispersible magnetite-reduced graphene oxide composites for arsenic removal. ACS Nano 4:3979–3986
7. Contreras D, Oviedo C, Valenzuela R, Freer J, Rojo K, Rodriguez J (2009) Tribromophenol degradation by a catechol-driven Fenton reaction. J Chil Chem Soc 54:141–143
8. Dubey S, Singh D, Misra RA (1998) Enzymatic synthesis and various properties of poly(catechol). Enzyme Microb Tech 23:432–437
9. Dong YH, Fujii H, Hendrich MP, Leising RA, Pan GF, Randall CR, Wilkinson EC, Zang Y, Que L, Fox BG, Kauffmann K, Munck E (1995) A high-valent nonheme iron intermediate structure and properties of $[Fe_2(.mu.-O)_2(5\text{-Me-TPA})_2](ClO_4)_3$. J Am Chem Soc 117:2778–2792
10. Dubey S, Singh D, Misra RA (1998) Enzymatic synthesis and various properties of poly(catechol). Enzyme Microbial Technology 23(7–8):432–437
11. Elhabiri M, Carrer C, Marmolle F, Traboulsi H (2007) Complexation of iron(III) by catecholate-type polyphenols. Inorg Chim Acta 360:353–359
12. Faure E, Falentin Daudre C, Jerome C, Lyskawa J, Fournier D, Woisel P, Detrembleur C (2013) Catechols as versatile platforms in polymer chemistry. Prog Polym Sci 38:236–270
13. Fang GD, Dionysiou DD, Al Abed SR, Zhou DM (2013) Superoxide radical driving the activation of persulfate by magnetite nanoparticles: Implications for the degradation of PCBs. App Catal B:

Environ 129:325–332

14. Feng Y, Wu D, Deng Y, Zhang T, Shih K (2016) Sulfate radical-mediated degradation of sulfadiazine by $CuFeO_2$ rhombohedral crystal-catalyzed peroxymonosulfate: synergistic effects and mechanisms. Environ Sci Technol 50:3119–3127
15. Gu L, Zhu N, Guo H, Huang S, Lou Z, Yuan H (2013) Adsorption and Fenton-like degradation of naphthalene dye intermediate on sewage sludge derived porous carbon. J Hazard Mater 246:145–153
16. Gao LZ, Zhuang J, Nie L, Zhang JB, Zhang Y, Gu N, Wang TH, Feng J, Yang DL, Perrett S, Yan X (2007) Intrinsic peroxidase-like activity of ferromagnetic nanoparticles. Nature Nanotech 2:577–583
17. Goncalves NPF, Minella M, Fabbri D, Calza P, Malitesta C, Mazzotta E, Prevot AB (2020) Humic acid coated magnetic particles as highly efficient heterogeneous photo-Fenton materials for wastewater treatments. Chem Eng J 390:124619
18. Gulley Stahl H, Hogan PA, Schmidt IIWL, Wall SJ, Buhrlage A, Bullen HA (2010) Surface complexation of catechol to metal oxides: an ATR-FTIR, adsorption, and dissolution study. Environ Sci Technol 44:4116–4121
19. He J, Yang X, Men B, Yu L, Wang D (2015) EDTA enhanced heterogeneous Fenton oxidation of dimethyl phthalate catalyzed by Fe_3O_4: Kinetics and interface mechanism. J Mol Catal A-Chem 408:179–188
20. He J, Yang X, Men B, Bi Z, Pu Y, Wang D (2014) Heterogeneous Fenton oxidation of catechol and 4-chlorocatechol catalyzed by nano-Fe_3O_4: Role of the interface. Chem Eng J 258:433–441
21. Hammouda SB, Adhoum N, Monser L (2015) Synthesis of magnetic alginate beads based on Fe_3O_4 nanoparticles for the removal of 3-methylindole from aqueous solution using Fenton process. J Hazard Mater 294:128–136
22. Hu XB, Liu BZ, Deng YH, Chen HZ, Luo S, Sun C, Yang P, Yang SG (2011) Adsorption and heterogeneous Fenton degradation of 17 alpha-methyltestosterone on nano Fe_3O_4/MWCNTs in aqueous solution. App Catal B: Environ 107:274–283
23. He Y, Huang L, Cai JS, Zheng XM, Sun SG (2010) Structure and electrochemical performance of nanostructured Fe_3O_4/carbon nanotube composites as anodes for lithium ion batteries. Electrochim Acta 55:1140–1144
24. Jho E, Singhal N, Turner S (2012) Tetrachloroethylene and hexachloroethane degradation in Fe(III) and Fe(III)-citrate catalyzed Fenton systems. J Chem Technol Biot 87:1179–1186
25. Jubb AM, Allen HC (2010) Vibrational Spectroscopic Characterization of Hematite, Maghemite, and Magnetite Thin Films Produced by Vapor Deposition. ACS Appl Mater Inter 2:2804–2812
26. Kang SH, Choi W (2009) Oxidative degradation of organic compounds using zero-valent iron in the presence of natural organic matter serving as an electron shuttle. Environ Sci Technol 43:878–883
27. Kong Y, Mu SF, Mao BW (2002) Synthesis of polycatechol with electrochemical activity and its properties. Chinese J Polym Sci 20:517–524

28. Li K, Zhao Y, Song C, Guo X (2017) Magnetic ordered mesoporous Fe_3O_4/CeO_2 composites with synergy of adsorption and Fenton catalysis. Appl Surf Sci 425:526–534
29. Luo W, Zhu L, Wang N, Tang H, Cao M, She Y (2010) Efficient removal of organic pollutants with magnetic nanoscaled $BiFeO_3$ as a reusable heterogeneous Fenton-Like catalyst. Environ Sci Technol 44:1786–1791
30. Li W, Wu X, Li S, Tang W, Chen Y (2018) Magnetic porous Fe_3O_4/carbon octahedra derived from iron-based metal-organic framework as heterogeneous Fenton-like catalyst. Appl Surf Sci 436:252–262
31. Leng Y, Guo W, Shi X, Li Y, Xing L (2013) Polyhydroquinone-coated Fe_3O_4 nanocatalyst for degradation of Rhodamine B based on sulfate radicals. Ind Eng Chem Res 52:13607–13612
32. Li GY, Huang KL, Jiang YR, Ding P, Yang DL (2008) Preparation and characterization of carboxyl functionalization of chitosan derivative magnetic nanoparticles. Biochem Eng J 40:408–414
33. Mondal P, Anweshan A, Purkait MK (2020) Green synthesis and environmental application of iron-based nanomaterials and nanocomposite: A review. Chemosphere 259
34. Melin V, Henriquez A, Freer J, Contreras D (2015) Reactivity of catecholamine-driven Fenton reaction and its relationships with iron(III) speciation. Redox Rep 20:89–96
35. Ma Z, Ren L, Xing S, Wu Y, Gao Y (2015) Sodium dodecyl sulfate modified $FeCo_2O_4$ with enhanced Fenton-like activity at neutral pH. J Phys Chem C 119:23068–23074
36. Magnacca G, Allera A, Montoneri E, Celi L, Benito DE, Gagliardi LG, Gonzalez MC, Mártire DO, Carlos L (2014) Novel magnetite nanoparticles coated with waste-sourced biobased substances as sustainable and renewable adsorbing materials. ACS Sustainable Chem Eng 2:1518–1524
37. Mercado DF, Cipollone M, González MC, Sánchez FH (2018) Yerba Mate applications: Magnetic response of powders and colloids of iron oxide nanoparticles coated with Ilex paraguariensis derivatives. J of Magn Magn Mater 462:13–21
38. Mercado DF, Weiss RG (2018) Polydimethylsiloxane as a Matrix for the Stabilization and Immobilization of Zero-Valent Iron Nanoparticles. J Braz Chem Soc 29:1427–1439
39. Mercado DF, Magnacca G, Malandrino M, Rubert A, Montoneri E, Celi L, Prevot AB, Gonzalez MC (2014) Paramagnetic iron-doped hydroxyapatite nanoparticles with improved metal sorption properties. a bioorganic substrates mediated synthesis. ACS Appl Mater Interfaces 6:3937–3946
40. Mercado DF, Caregnato P, Villata1 LS, Gonzalez MC (2018) Ilex paraguariensis extract-coated magnetite nanoparticles: a sustainable nano-adsorbent and antioxidant. J Inorg Organo met P 28:519–527
41. Noorjahan A, Kumari VD, Subrahmanyam A, Panda L (2005) Immobilized Fe(III)-HY: an efficient and stable photo-Fenton catalyst. App Catal B: Environ 57:91–298
42. Niu H, Zhang D, Zhang S, Zhang X, Meng Z (2011) Humic acid coated Fe_3O_4 magnetic nanoparticles as highly efficient Fenton-like catalyst for complete mineralization of sulfathiazole. J Hazard Mater 190:559–565

43. Pu J, Shen L, Zhu S, Wang J, Zhang W, Wang Z (2014) Fe_3O_4@C core-shell microspheres: synthesis, characterization, and application as supercapacitor electrodes. J Solid State Electr 18:1067–1076
44. Rahhal S, Richter HW (1988) Reductionof hydrogen-peroxide by the frrrous iron chelate of diethylenetriamine-N,N,N',N",N"- pentaacetate. J Am Chem Soc 110:3126–3133
45. Slikboer S, Grandy L, Blair SL, Nizkorodov SA, Smith RW, Al-Abadleh HA (2015) Formation of light absorbing soluble secondary organics and insoluble polymeric particles from the dark reaction of catechol and guaiacol with Fe(III). Environ Sci Technol 49:7793–7801
46. Wang J, Cao ZF, Ren H, Yu C, Wang S, Li L, Zhong H (2020) Reactivation of Fenton catalytic performance for Fe_3O_4 catalyst: optimizing the cyclic performance by low voltage electric field. Appl Surf Sci 500
47. Wang N, Zhu L, Wang D, Wang M, Lin Z, Tang H (2010) Sono-assisted preparation of highly-efficient peroxidase-like Fe_3O_4 magnetic nanoparticles for catalytic removal of organic pollutants with H_2O_2. Ultrason. Sonochem 17:526–533
48. Wang W, Liu Y, Li T, Zhou M (2014) Heterogeneous Fenton catalytic degradation of phenol based on controlled release of magnetic nanoparticles. Chem Eng J 242:1–9
49. Wang W, Wang Y, Liu Y, Li T (2012) Synthesis of novel pH-responsive magnetic nanocomposites as highly efficient heterogeneous Fenton catalysts. Chem Lett 41:897–899
50. Xu CJ, Xu KM, Gu HW, Zheng RK, Liu H, Zhang XX, Guo ZH, Xu B (2004) Dopamine as a robust anchor to immobilize functional molecules on the iron oxide shell of magnetic nanoparticles. J Am Chem Soc 126:9938–9939
51. Xiang HL, Ren GK, Zhong YJ, Xu DH, Zhang ZY, Wang XL, Yang XS (2021) Fe_3O_4@C nanoparticles synthesized by in situ solid-phase method for removal of methylene blue. Nanomaterials 11
52. Xiao J, Wang C, Lyu SS, Liu H, Jiang CC, Lei YM (2016) Enhancement of Fenton degradation by catechol in a wide initial pH range. Sep Purif Technol 169:202–209
53. Xie G, Xi P, Liu H, Chen F, Huang L, Shi Y, Hou F, Zeng Z, Shao C, Wang J (2012) A facile chemical method to produce superparamagnetic graphene oxide-Fe_3O_4 hybrid composite and its application in the removal of dyes from aqueous solution. J Mater Chem 22:1033–1039
54. Xu L, Wang J (2012) Fenton-like degradation of 2,4-dichlorophenol using Fe_3O_4 magnetic nanoparticles. App Catal B: Environ 123:117–126
55. Xue X, Hanna K, Abdelmoula M, Deng N (2009) Adsorption and oxidation of PCP on the surface of magnetite: Kinetic experiments and spectroscopic investigations. App Catal B: Environ 89:432–440
56. Ye Q, Zhou F, Liu W (2011) Bioinspired catecholic chemistry for surface modification. Chem Soc Rev 40:4244–4258
57. Zubir NA, Yacou C, Motuzas J, Zhang X, da Costa JCD (2014) Structural and functional investigation of graphene oxide-Fe_3O_4 nanocomposites for the heterogeneous Fenton-like reaction. Sci Rep 4
58. Zhang JW, Azam MS, Shi C, Huang J, Bin B, Liu QX, Zeng HB (2015) Poly (acrylic acid) functionalized magnetic graphene oxide nanocomposite for removal of methylene blue. Rsc Adv

5:32272–32282

59. Zhang X, He M, Liu JH, Liao R, Zhao L, Xie J, Wang R, Yang ST, Wang H, Liu Y (2014) Fe_3O_4@C nanoparticles as high-performance Fenton-like catalyst for dye decoloration. Chinese Sci Bull 59:3406–3412
60. Zhang X, Ding Y, Tang H, Han X, Zhu L, Wang N (2014) Degradation of bisphenol A by hydrogen peroxide activated with $CuFeO_2$ microparticles as a heterogeneous Fenton-like catalyst: Efficiency, stability and mechanism. Chem Eng J 236:251–262

Schemes

Schemes are in the Supplementary Files.

Figures

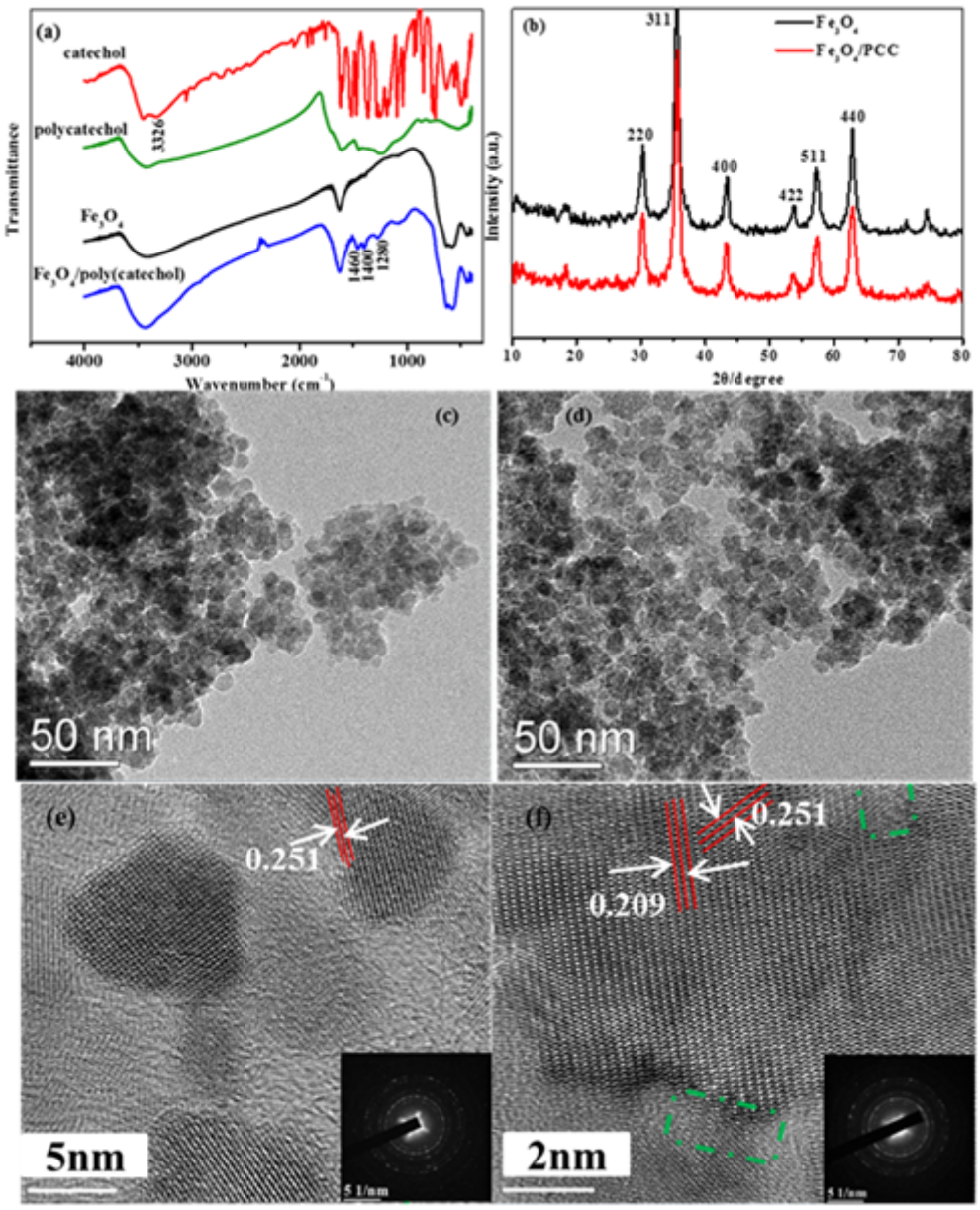

Figure 1

(a)FTIR spectra of catechol, poly(catechol), Fe3O4 and Fe3O4/PCC MNPs; (b) X-ray powder diffraction pattern of Fe3O4/PCC and Fe3O4 MNPs; TEM image of Fe3O4 MNPs (c) and Fe3O4/PCC MNPs (d); HRTEM image of Fe3O4 MNPs (e) and Fe3O4/PCC MNPs.

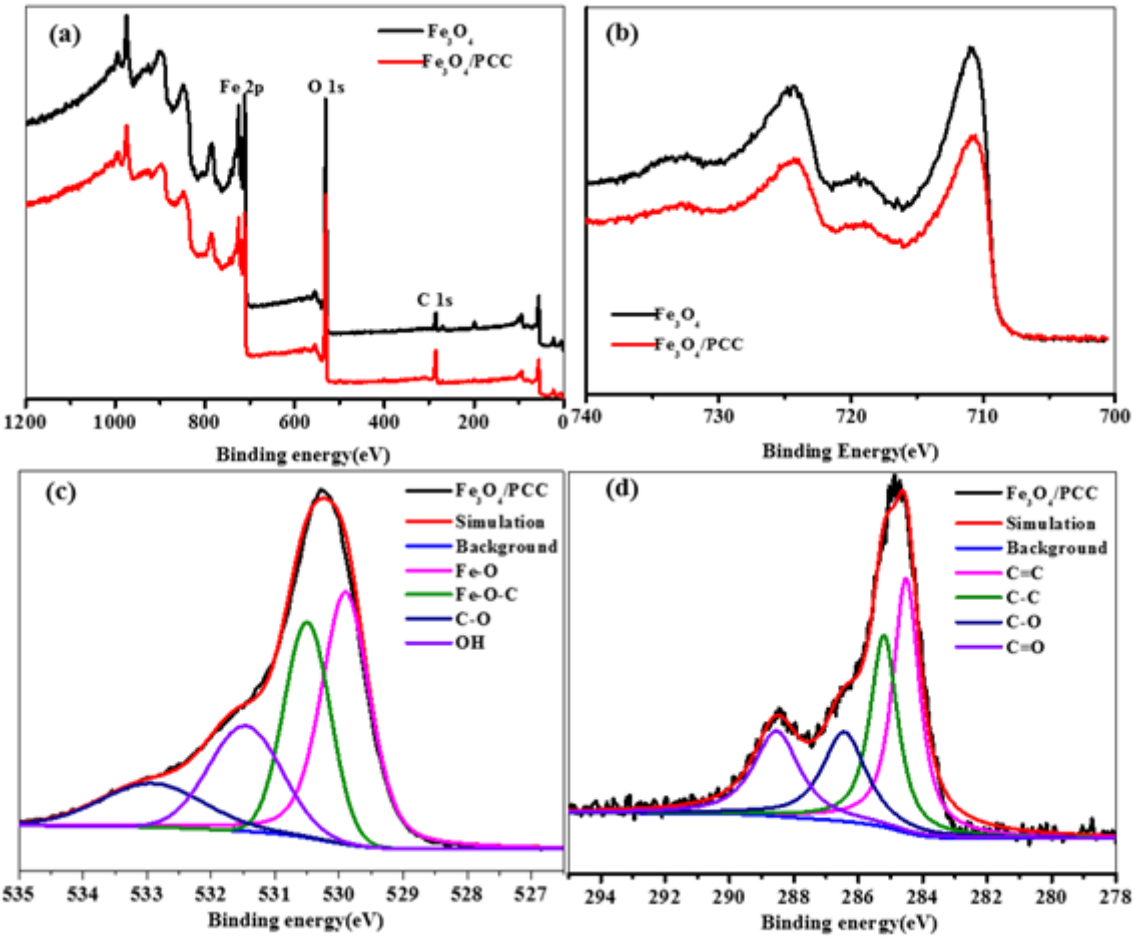

Figure 2

Wide scan XPS spectra (a) and high resolution Fe 2p spectra (b) of Fe3O4 and Fe3O4/PCC MNPs; (c) Fe 2P spectra of Fe3O4; (d) Fe 2P spectra of Fe3O4/PCC; O 1s XPS spectra (e) and C 1s XPS spectra (f) of Fe3O4/PCC MNPs.

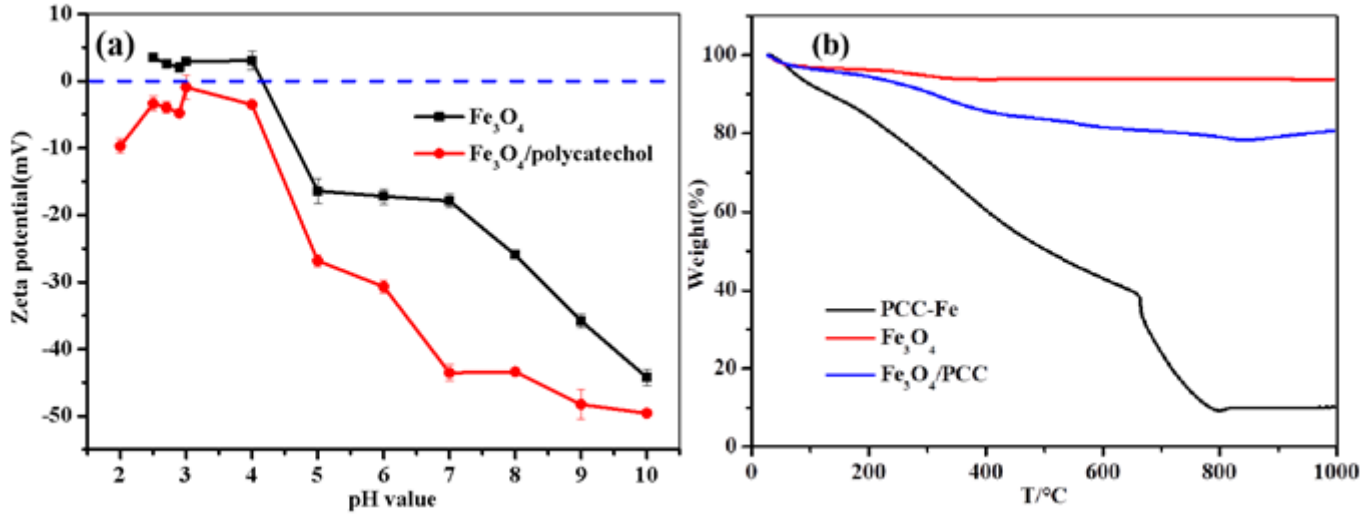

Figure 3

(a) Zeta potential of Fe3O4 and Fe3O4/PCC MNPs at various pH values; (b) TGA curves of poly(catechol)-Fe, Fe3O4 and Fe3O4/PCC MNPs.

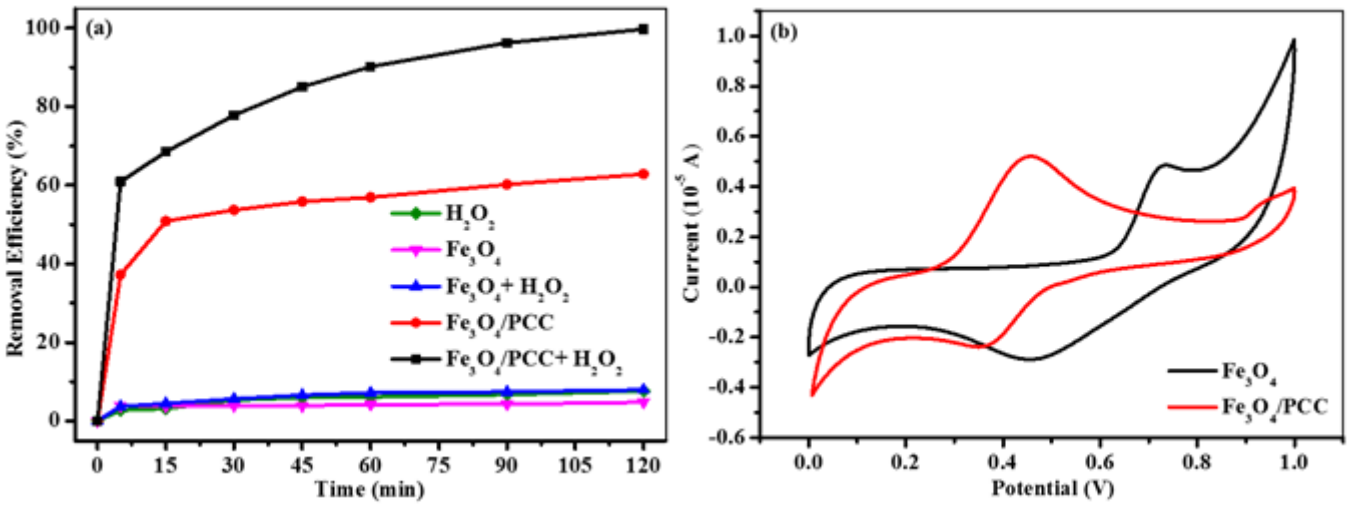

Figure 4

(a) Removal curves of MB under different conditions at pH 6.0 ([Fe3O4/PCC] = 1.0 g L-1, [Fe3O4] = 1.0 g L-1, [H2O2]0 = 40.0 mM, [MB]0 = 0.1 mM, T = 30 °C); (b) Cyclic voltammetry scans with Fe3O4/PCC and Fe3O4 modified glassy carbon electrodes in a 0.1 M Na2SO4 aqueous solution at pH 6.0.

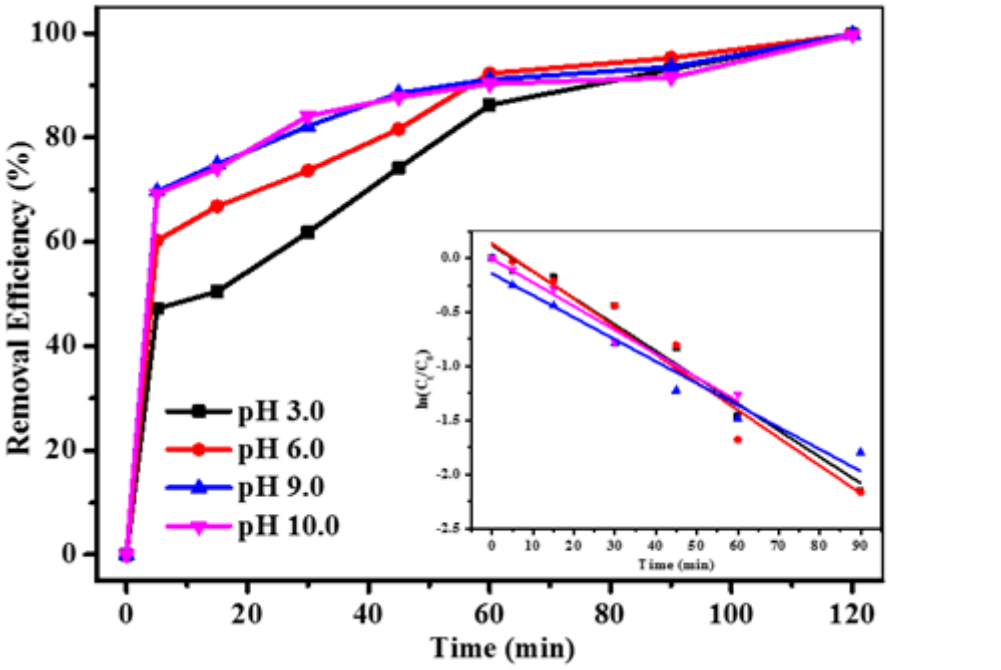

Figure 5

The effect of initial pH value of MB solution on the removal efficiency of MB degraded using Fe3O4/PCC MNPs as catalyst, inset is pseudo-first-order kinetics of MB degradation ([Fe3O4/PCC] = 1.0 g L-1, [H2O2]0 = 40 mM, [MB]0 = 0.1 mM, T = 30 °C)

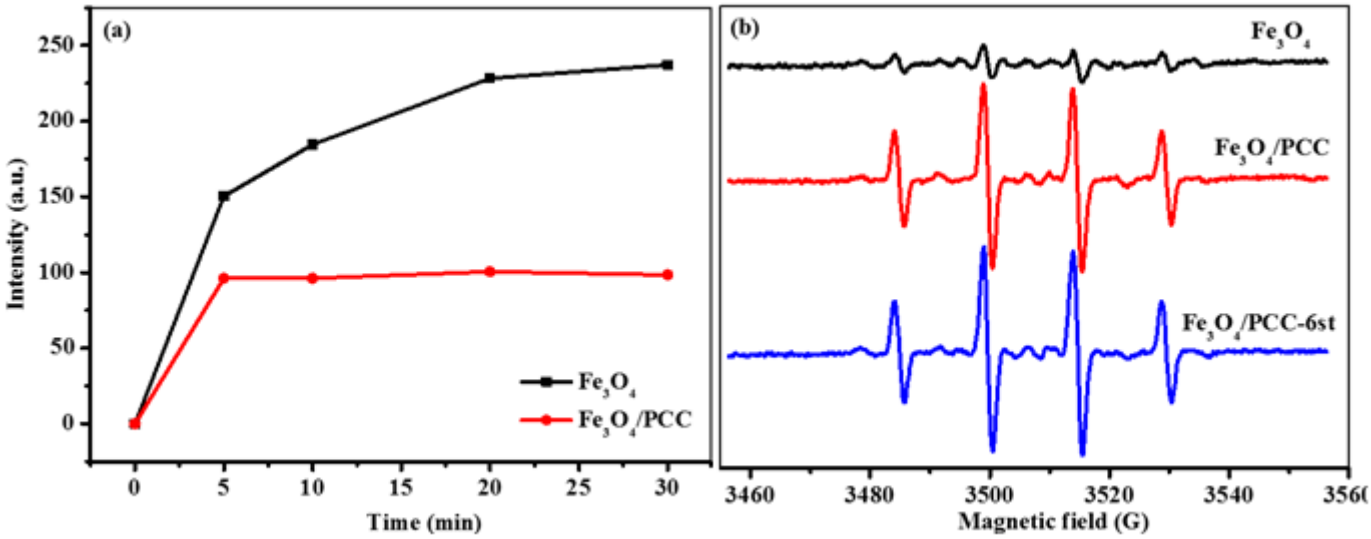

Figure 6

(a) Fluorescence intensity of NBD-Cl-•O2- (b) DMPO spin-trapping ESR spectra of •OH radicals in heterogeneous Fenton reaction with Fe3O4, Fe3O4/PCC and Fe3O4/PCC-6st as catalyst ([catalyst] = 1.0 g L-1, [H2O2]0 = 40 mM, [DMPO] = 500 mM, [NBD-Cl] = 2.0 mM, pH 6.0, T = 30 °C, t = 20 min)

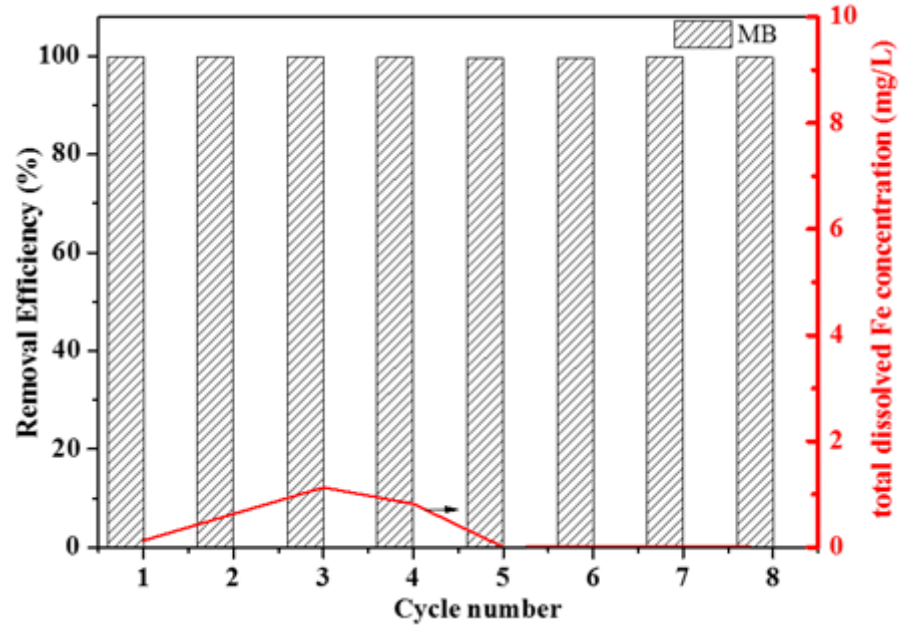

Figure 7

Removal efficiency of MB with histogram and total dissolved Fe concentration in each cycle was expressed by curve. ([Fe3O4/PCC] = 1.0 g L-1, [H2O2]0 = 40 mM, [MB]0 = 0.1 mM, pH = 6.0, T = 30 °C, t = 120 min)

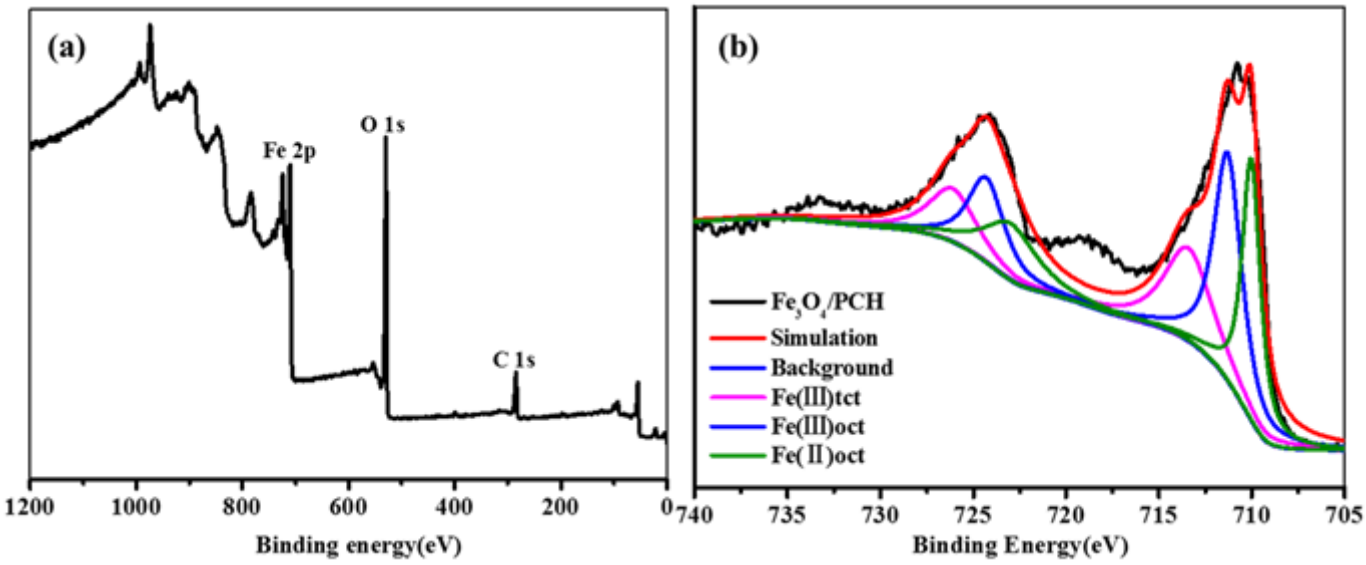

Figure 8

XPS spectra of used Fe3O4/PCC MNPs. (a) Wide scan XPS spectra, (b) XPS curve fit of Fe 2p.

Supplementary Files

This is a list of supplementary files associated with this preprint. Click to download.

- SupplementaryMaterial.doc
- floatimage1.png
- floatimage11.png